



Effect of Prolonged Exposure to High Temperature Air on Physical Characteristics of a Powder Metallurgy Composite Solid Lubricant

Malcolm K. Stanford
Glenn Research Center, Cleveland, Ohio

La’Nita D. Ward
Spelman College, Atlanta, Georgia

Christopher DellaCorte
Glenn Research Center, Cleveland, Ohio

NASA STI Program . . . in Profile

Since its founding, NASA has been dedicated to the advancement of aeronautics and space science. The NASA Scientific and Technical Information (STI) program plays a key part in helping NASA maintain this important role.

The NASA STI Program operates under the auspices of the Agency Chief Information Officer. It collects, organizes, provides for archiving, and disseminates NASA's STI. The NASA STI program provides access to the NASA Aeronautics and Space Database and its public interface, the NASA Technical Reports Server, thus providing one of the largest collections of aeronautical and space science STI in the world. Results are published in both non-NASA channels and by NASA in the NASA STI Report Series, which includes the following report types:

- **TECHNICAL PUBLICATION.** Reports of completed research or a major significant phase of research that present the results of NASA programs and include extensive data or theoretical analysis. Includes compilations of significant scientific and technical data and information deemed to be of continuing reference value. NASA counterpart of peer-reviewed formal professional papers but has less stringent limitations on manuscript length and extent of graphic presentations.
- **TECHNICAL MEMORANDUM.** Scientific and technical findings that are preliminary or of specialized interest, e.g., quick release reports, working papers, and bibliographies that contain minimal annotation. Does not contain extensive analysis.
- **CONTRACTOR REPORT.** Scientific and technical findings by NASA-sponsored contractors and grantees.

- **CONFERENCE PUBLICATION.** Collected papers from scientific and technical conferences, symposia, seminars, or other meetings sponsored or cosponsored by NASA.
- **SPECIAL PUBLICATION.** Scientific, technical, or historical information from NASA programs, projects, and missions, often concerned with subjects having substantial public interest.
- **TECHNICAL TRANSLATION.** English-language translations of foreign scientific and technical material pertinent to NASA's mission.

Specialized services also include creating custom thesauri, building customized databases, organizing and publishing research results.

For more information about the NASA STI program, see the following:

- Access the NASA STI program home page at <http://www.sti.nasa.gov>
- E-mail your question via the Internet to help@sti.nasa.gov
- Fax your question to the NASA STI Help Desk at 301-621-0134
- Telephone the NASA STI Help Desk at 301-621-0390
- Write to:
NASA STI Help Desk
NASA Center for AeroSpace Information
7121 Standard Drive
Hanover, MD 21076-1320



Effect of Prolonged Exposure to High Temperature Air on Physical Characteristics of a Powder Metallurgy Composite Solid Lubricant

Malcolm K. Stanford
Glenn Research Center, Cleveland, Ohio

La'Nita D. Ward
Spelman College, Atlanta, Georgia

Christopher DellaCorte
Glenn Research Center, Cleveland, Ohio

National Aeronautics and
Space Administration

Glenn Research Center
Cleveland, Ohio 44135

Acknowledgments

Thank you to R.J. Bruckner and B.J. Puleo for performing regression analyses, to D.J. Dixon and T.R. McCue for SEM analysis, to J.A. Buehler and M.S. McQuater for metallographic specimen preparation, to A.R. Palczer for surface area analysis measurements, to B.J. Edmonds and V. Lukaszewicz for setting up heat exposure experiments, to R.G. Garlick for XRD analyses, and to E.J. Opila and J.L. Smialek for highly valued technical discussions.

This report is a formal draft or working paper, intended to solicit comments and ideas from a technical peer group.

This report contains preliminary findings, subject to revision as analysis proceeds.

Level of Review: This material has been technically reviewed by technical management.

Available from

NASA Center for Aerospace Information
7121 Standard Drive
Hanover, MD 21076-1320

National Technical Information Service
5285 Port Royal Road
Springfield, VA 22161

Available electronically at <http://gltrs.grc.nasa.gov>

Effect of Prolonged Exposure to High Temperature Air on Physical Characteristics of a Powder Metallurgy Composite Solid Lubricant

Malcolm K. Stanford
National Aeronautics and Space Administration
Glenn Research Center
Cleveland, Ohio 44135

La'Nita D. Ward
Spelman College
Atlanta, Georgia 30314

Christopher DellaCorte
National Aeronautics and Space Administration
Glenn Research Center
Cleveland, Ohio 44135

Abstract

The effects of exposure to high temperatures has been investigated for PM300, a powder metallurgy composite solid lubricant composed of nickel-chromium, chromia, silver, and an alkaline earth fluoride. Specimens were exposed to 500 and 650 °C in air for time intervals up to 5,000 hr and then examined for changes in their microstructure, mass, size, and hardness. After heat exposure, the microstructure showed formation of precipitates within the nickel-chromium constituent, with a corresponding increase in mass, size, and hardness. The percent increase in mass and size followed a logarithmic curve, which provides guidance for heat treatment parameters.

Introduction

PM304 is a powder metallurgy version of PS304 composite solid lubricant composed of 60 w/o Ni-20Cr (80 w/o Ni – 20 w/o Cr), 20 w/o Cr₂O₃, 10 w/o Ag, and 10 w/o eutectic BaF₂-CaF₂ (ref. 1). This composite material is very stable thermo-chemically and, therefore, used in high temperature applications such as industrial furnace conveyors where conventional oil-based lubricants and traditional solid lubricants (e.g., molybdenum disulfide and graphite) are not functional. The Ni-20Cr and Cr₂O₃ constituents in this material provide hard phases for wear resistance. The Ag and BaF₂-CaF₂ phases provide solid lubrication by deforming plastically in shear through a range of operating temperatures. The Ag constituent provides lubrication from room temperature to about 550 °C, while the BaF₂-CaF₂ is active as a lubricant from about 450 to above 900 °C (ref. 2). A forthcoming publication provides an excellent review of the historical development of PM300 as well as a report on its tribological performance (ref. 3).

Bemis et al. investigated the effect of high temperature exposure on the microstructure and tribological performance of PM212, a cold isostatic pressed, liquid phase sintered precursor to PM300 that was composed of 70 w/o Cr₃C₂, 15 w/o BaF₂-CaF₂, and 15 w/o Ag (ref. 4). This study determined that the mass and thickness of PM212 increased with increasing exposure time. After 100 hr of exposure, no further increase in thickness was observed. The data indicated that the rate of mass and thickness increase was higher for thicker specimens indicating that the changes were due to diffusion of oxygen into the material. However, the difference in the oxidation behaviors of PM212 and PM300 are unknown and should be studied independently.

The current investigation was initiated after a preliminary study of the effects of long-term exposure of PM300-type bushings to 650 °C air demonstrated that the material continued to grow beyond 100 hr of

exposure. The data showed that after 9,000 hr in 650 °C air, the inner diameter grew approximately 5 percent, the outer diameter grew by approximately 9 percent and the thickness decreased by about 4 percent. However, it was unclear whether this behavior was influenced by the shape and size of the component (i.e., the reduction in thickness may have been restricted because the material was confined to the cylindrical geometry of the specimen). Therefore, the current investigation used specimens sectioned from whole bushings so that the ends were not confined. The purpose of this investigation was to characterize the physical changes that occur in PM300 powder metallurgy composite with prolonged exposure to high temperatures to better understand the observed dimensional changes.

Experimental Procedures

Materials

PM304 is composed of nickel–chromium (Ni-20 w/o Cr), chromia (Cr_2O_3), silver, and eutectic barium fluoride–calcium fluoride (BaF_2 -32 w/o CaF_2) powders. The physical characteristics of the precompaction powder blend are listed in table 1. Powder size, surface area, density, angle of repose, and flow measurements were performed at 21 °C and nominally 52 percent relative humidity according to standard test procedures (refs. 5 to 10). The powder did not flow through a Hall or Carney flowmeter funnel (ref. 11).

Methods

Right cylindrical powder metallurgy compacts (35 mm I.D. \times 45 mm O.D. \times 19 mm height) were prepared by uniaxial double-action cold pressing. The compacts were then loaded into a furnace at 1100 °C for 20 min in a dry hydrogen atmosphere to enable liquid phase sintering via melting of the silver and eutectic fluoride phases. The approximate melting temperatures and purity levels of the constituent materials, based on the suppliers' data, are listed in table 2. Finished bushings are shown in figure 1. The sintered density (typically about 6 g/cm³) is approximately 85 percent of theoretical density (7 g/cm³) with very little shrinkage from the green state to the fully sintered material.

Several bushings were sectioned diametrically into sixteenths, resulting in arc-shaped sections approximately 5 mm thick, 18 mm wide, and 19 mm in height. These specimens were ultrasonically cleaned in methanol, rinsed in deionized water, and dried at 150 °C under a moderate vacuum. The thickness and mass of each specimen was measured and recorded (typically 4.5 mm and 6.5 g, respectively). Specific surface area was measured by the BET method (ref. 12).

Each specimen was placed in an array on a ceramic fixture and loaded into a furnace. Tests were run at 500 and 650 °C. An adjacent control specimen was retained and set aside at room temperature. The treated specimens were removed from the furnace sequentially at predetermined time intervals from 1 to 5,000 hr. Up to 10 hr, specimens were removed in 1 hr increments. Changes in specimen size and mass were recorded. The specimens were then prepared for metallographic examination with a fluorescent mounting medium such that the pores in the specimen were filled with epoxy. Microindentation hardness was measured in several locations on each specimen with a Vickers pyramidal diamond indenter applying a test load of 300 gf for 5 sec (ref. 13). Microstructural changes due to heat exposure were noted.

Results and Discussion

Figure 2 shows photomicrographs of PM300 cross sections with labels indicating the Ni-20Cr, Cr_2O_3 , and Ag constituents. The silver and fluorides melt during the sintering step of compact preparation (liquid phase sintering) and are drawn to the spaces between adjacent nickel-chromium and chromium oxide particles, as shown in the figure. More specifically, the silver phase tends to melt and adhere to (wet) the Ni-20Cr particles, while the fluorides tend to wet the chromia particles. The top two photomicrographs in figure 2 show the same area on a nonheat treated specimen. Figure 2(a) is a

brightfield image wherein the Ni-20Cr particles are medium grey, the Ag particles are light grey and the Cr₂O₃ particles are black. The BaF₂-CaF₂ particles are optically transparent and look black in the image (surrounding the Cr₂O₃ particles). However, pores also look flat black in brightfield photomicrographs so they are very difficult to distinguish from other microstructural features (especially the fluorides). Therefore, the specimens were prepared for metallographic examination with an epoxy mounting medium incorporating a fluorescent dye. To maximize infiltration of the specimen, the epoxy was poured around the specimens under a moderate vacuum and then cured under pressure. The photomicrograph in figure 2(b) was taken through a fluorescent filter with polarized light so that the pores (infiltrated with fluorescing mounting media) are green in the image. Comparing figures 2(a) and (b), the pores (green) can now be distinguished from the rest of the microstructure. Figures 2(c) and (d) are SEM images from a different area on the same specimen. The secondary electron image (fig. 2(c)) emphasizes the topographical features in the microstructure so that pores (black) are easily distinguished from ceramic phases. The backscattered electron image (fig. 2(d)) emphasizes the average atomic mass of the different phases so that the fluorides (medium grey) are somewhat more distinct than the chromia particles (dark grey). The white Ag phase filling the gaps between adjacent Ni-20Cr particles is more pronounced. Analysis of this irregular microstructure has been facilitated with the wide variety of available microscopic techniques.

The tendency for the silver to wet the Ni-20Cr particles and for the fluorides to wet the Cr₂O₃ particles is thought to be due to the similarity in surface free energy for the two material classes. That is to say, for chemically similar phases, wetting of a solid phase by a liquid phase is more thermodynamically favorable than for chemically dissimilar phases. This is because the solid-liquid interface energy tends to be less than the sum of the solid-vapor and liquid-vapor interface energies thereby giving the liquid phase a greater propensity to spread than to evaporate or diffuse into the solid. Likewise, for dissimilar material phases, the solid-liquid interface energy tends to be high, discouraging wetting. More specifically, liquid metals (e.g., silver) tend not to wet ionic solids (e.g., chromia) and ionic liquids (like fluorides) wet, but tend not to spread on, metals (like Ni-20Cr) in inert atmospheres (refs. 14 and 15).

After exposure to high temperature air, the Ni-20Cr phase within the composite tends to develop precipitates, consistent with findings for the plasma spray version of this material exposed to similar conditions (refs. 16 to 18). Figure 3 shows changes in the microstructure of the composite after exposure to 500 and 650 °C for 100 hr. The precipitates in the Ni-20Cr phase are indicated in the photomicrograph.

Few, if any, precipitates are visible on the specimen exposed to 500 °C for 100 hr. After 500 hr, however, precipitates are also visible on both specimens, as shown in figure 4. It is evident, therefore, that the onset of this precipitate formation takes place sooner at higher temperatures.

X-ray diffraction of a specimen exposed to 650 °C for 1,000 hr indicated formation of NiO and a NiCr₂O₄ spinel, consistent with thermodynamic equilibrium calculations. Since Cr₂O₃ was present in the pre-oxidized material, it is unclear if it was also generated due to oxidation. However, the Cr₂O₃ in the equilibrium composition in the high temperature environment is likely to be converted to the spinel.

Photomicrographs from a cross-section of a specimen exposed to 500 °C for 5,000 hr are shown in figure 5. Some of the precipitates in the cross section are highlighted in figure 5(a). Energy-dispersive spectrometry (EDS) analysis revealed that the precipitates were chromium-rich. These features were previously thought to be Cr₂O₃ (refs. 16 and 19) but are likely composed of oxides or spinels of Cr and Ni. The spectra from each feature labeled in figure 5(b) are shown in figure 6. The spectra in figures 6(a) and (b) indicate a higher concentration of Cr than Ni, while the opposite is true for the spectrum in figure 6(c). The feature this spectrum represents appears to be a void. It is possible that a precipitate was formed here that was not retained during metallographic preparation or that the feature is a Kirkendall void (ref. 20) with a small precipitate on the inner wall. An elemental dot map of some of the features in figure 5(b) is shown in figure 7. The dot map shows a concentration of Cr and O along with a depletion of Ni across the precipitate. Feature A from figure 5(b) was analyzed with an elemental line scan, as shown in figure 8. The photomicrograph (fig. 8(a)) was captured using a 6 kV electron accelerating voltage (versus 20 to 25 kV used typically) so that surface features are more dominant and the precipitate is more

distinct. The line scan (fig. 8(b)) also indicates that the precipitate is chromium-rich. It should be noted that there is a distinct difference in the morphology of the faceted chromia used in the precompaction material feedstock and the rounded, irregular precipitates. Further work is needed to characterize these precipitates and the mechanisms by which they evolve.

The percent mass change is plotted against exposure time at 500 and 650 °C in figure 9. Clearly, the magnitude and rate of mass change are temperature dependent. The data were compared to parabolic, quadratic, and logarithmic regression curves, consistent with classical oxidation kinetics (refs. 21 to 22). The data were found to be best described by a function of the natural logarithm of exposure time. Therefore, the rate of mass change \dot{m} is determined using the derivative

$$\dot{m} = \frac{d}{dt} \ln(t) = \frac{1}{t},$$

which indicates that the rate of mass change decreases as a linear function of time. At 650 °C, the regression model was given by $y = -0.941 + 1.87 \ln(t)$, while at 500 °C, it was $y = -1.74 + 1.08 \ln(t)$. This is an unexpected result since internal oxidation occurs by nucleation and growth mechanisms, which observe sigmoidal oxidation kinetics (refs. 21 to 23). In addition, logarithmic oxidation behavior is normally consistent with bulk metal oxidation observed at ambient or slightly elevated temperatures (refs. 24 to 25). For logarithmic kinetics to take place, it is possible that one of the coating constituents (BaF₂-CaF₂ for example) catalyzes the reaction during the initial stages. It has been observed that the precipitates tend to form where the Ni-20Cr is in contact with a BaF₂-CaF₂ phase, as mentioned in earlier work (ref. 17). Furthermore, the precipitates do not form when BaF₂-CaF₂ is not present (ref. 16). The role BaF₂-CaF₂ plays in the observed reaction is not well understood at this time and needs further study.

Based on the starting composition and the equilibrium chemistry at high temperature, the studied material will undergo a weight gain of approximately 20 percent. At this point, all of the Ni and Cr will be converted to an oxide or spinel. The estimated equilibrium weight gain may be compared to any observed weight gain to predict parameters such as the oxidized fraction of a particular starting constituent.

Figure 10 shows the percent dimensional change plotted with respect to exposure time. The best model of the growth behavior was also a function of the natural logarithm of exposure time. The regression model at 650 °C was given by $y = 2.02 + 0.959 \ln(t)$, and $y = 1.18 + 0.567 \ln(t)$ at 500 °C. Incidentally, the ratio of the growth rate coefficients in the two equations is $0.959/0.567 \approx 1.7$; the same is true for the rate coefficients in the mass increase equations ($1.87/1.08 \approx 1.7$). Also note that about 50 percent of the observed material dimensional change occurs within the first 10 hr of exposure to high temperature air and 85 percent of the dimensional change has occurred within approximately 250 hr. For component design, it may be tempting to extrapolate to predict maximum growth based on these models. However, the models do not account for the fact that growth is usually counteracted by dynamic wear processes and they imply that growth continues indefinitely. The effects of prior oxidation on the continued oxidation of the material are unknown.

Clearly, the mass and dimensional increases in this material are due to oxidation. The rate of mass increase, however, is not the same as the rate of thickness increase at a given temperature. Since mass increases as a function of material volume (the product xyz), and thickness is only a function of x , all of the material response information may not be expressed by the thickness measurement alone. Moreover, due to the technique (uniaxial hot pressing) used to fabricate the studied material; there is inherent anisotropy that results in different dimensional growth rates, depending upon the measurement axis. The thickness rate coefficients are, in fact, approximately half the mass coefficients.

To better compare the oxidation kinetics, the normalized mass and dimension increases are plotted with respect to the logarithm of exposure time in figure 11. This plot reinforces the fact that the rate of oxidation is higher at 650 °C. It is also clear that the rate of mass increase (given by the slope of the line) is greater than the rate of thickness increase, regardless of temperature. Since the rate of dimensional change is 70 percent higher at 650 than at 500 °C, some information relevant to heat treatment may be

gleaned from this result. For example, if dimensional stability is important to the application, a heat treatment at a temperature higher than the operating temperature for the application may be an effective way to stabilize growth of the material. Also, if high loads resulting in thermal spikes are expected, the microstructure should be heat treated thoroughly to prevent excessive growth. However, when high wear rates are expected at temperatures at or below the heat treatment temperature, shorter heat treatments may be employed as well as lower heat treatment temperatures. The rate and magnitude of the oxidation reaction is controlled by temperature, but both appear to saturate at some level at either temperature. The relatively poor fit of the data to the regression curves at shorter time intervals indicates that there is perhaps more than a single rate in effect during the initial oxidation reaction. As mentioned previously, during nucleation of oxide precipitates, the reaction is expected to occur at a lower rate. However, the apparent catalytic effect the BaF₂-CaF₂ phase has on oxidation may enable multiple mechanisms to control the kinetics at shorter time intervals, which would significantly alter reaction rates.

Figure 12 shows the change in the microstructure of the material after exposure to 500 °C for 250 and 500 hr. There is a slight indication of film on the Ni-20Cr constituent in figures 12(c) and (d). Figure 13 shows the evolution of this film after the material was exposed to 650 °C for 3,000 hr. Chemical analysis found the film to be composed of nickel, chromium, and oxygen, likely NiO, Cr₂O₃ or NiCr₂O₄. The film is an indication of oxidation at the surface of the Ni-20Cr particles, possibly by the outward diffusion of metal atoms, as well as diffusion of oxygen into the Ni-20Cr solid solution where precipitates are formed (ref. 26). The fact that both internal and external oxidation mechanisms have been observed in the studied material system is intriguing. One might speculate that, since the film formation is not appreciable until after longer heat exposure times, the two mechanisms operate in series with precipitate formation preceding external oxidation enabled by chemical reaction with the BaF₂-CaF₂ phase. However, this reaction is not well understood at this time and requires further study.

The microindentation hardness of PM300 with respect to exposure time is plotted in figure 14. The dashed lines indicate the range of control sample (non-heat treated) data. The data suggest that the hardness of the material generally increases with increasing time of exposure to high temperature air. The error bars, representing the standard deviation of measurements at each condition, indicate that there is no significant difference in the hardness of the material with exposure to 500 or 650 °C. The increase in hardness due to temperature exposure is also consistent with the formation of relatively hard oxide-compounds in the softer Ni-20Cr solid solution.

Conclusions

This purpose of this investigation was to characterize the physical changes in PM300 powder metallurgy solid lubricant material. Based on the results of this study, the following conclusions were made:

- The material develops precipitates within the nickel-chromium constituent after exposure to high temperature air.
- The composition of the precipitates is chromium and oxygen rich, most likely a combination of oxides and spinels of nickel and chromium.
- The percent mass change and percent dimensional change in the material can be described as a function of the natural logarithm of exposure time.
- For moderate loads and steady temperatures, a shorter or lower temperature heat treatment may be used. For high loads or where high thermal gradients may be encountered, the microstructure should be heat treated for more than 250 hr to ensure dimensional stability.
- Heat treatment at a higher temperature than the operating temperature may be an effective route to obtaining a dimensionally stable microstructure for this material in a shorter time period.
- The hardness of the material increases with increasing exposure to high temperature air, indicating the formation of an oxide precipitation hardened phase.
- Further work is needed to characterize the oxidation kinetics in this material.

References

1. C. DellaCorte and B.J. Edmonds, "Self-lubricating Composite Containing Chromium Oxide," U.S. Patent no. 5,866,518, February 2, 1999.
2. D.L. Deadmore and H.E. Sliney, "Hardness of CaF₂ and BaF₂ Solid Lubricants at 25 to 670 °C," 1987, NASA Technical Memorandum 88979, National Technical Information Service, Springfield, VA.
3. D.R. Striebing, M.K. Stanford, C. DellaCorte, and A.M. Rossi, "Tribological Performance of PM300 Solid Lubricant Bushings for High Temperature Applications," to be published as a NASA Technical Memorandum, National Technical Information Service, Springfield, VA.
4. K. Bemis, M.S. Bogdanski, C. DellaCorte, and H.E. Sliney, "The Effect of Prolonged Exposure to 750 °C Air on the Tribological Performance of PM212," 1994, NASA Technical Memorandum 106472, National Technical Information Service, Springfield, VA.
5. ASTM Test Method B214-99, "Standard Test Method for Sieve Analysis of Metal Powders," 1999, Annual Book of ASTM Standards, vol. 02.05, West Conshohocken, PA: American Society for the Testing of Materials.
6. ASTM Test Method B212-99, "Standard Test Method for Determination of Apparent Density of Free-Flowing Metal Powders Using the Hall Flowmeter Funnel," 2001, Annual Book of ASTM Standards, vol. 02.05, West Conshohocken, PA: American Society for the Testing of Materials.
7. ASTM Test Method B527-93(2001)e1, "Standard Test Method for Determination of Tap Density of Metallic Powders and Compounds," 2001, Annual Book of ASTM Standards, vol. 02.05, West Conshohocken, PA: American Society for the Testing of Materials.
8. ASTM Test Method C1444-00, "Standard Test Method for Measuring the Angle of Repose of Free-Flowing Mold Powders," 2003, Annual Book of ASTM Standards, vol. 15.01, West Conshohocken, PA: American Society for the Testing of Materials.
9. ASTM Test Method B213-97, "Standard Test Method for Flow Rate of Metal Powders, Annual Book of ASTM Standards," 1998, vol. 02.05, West Conshohocken, PA: American Society for the Testing of Materials.
10. ASTM B922-02, "Standard Test Method for Metal Powder Specific Surface Area by Physical Adsorption," 2003, Annual Book of ASTM Standards, vol. 02.05, West Conshohocken, PA: American Society for the Testing of Materials.
11. ASTM B417-00, "Standard Test Method for Apparent Density of Non-Free-Flowing Metal Powders Using the Carney Funnel," 2003, Annual Book of ASTM Standards, vol. 02.05, West Conshohocken, PA: American Society for the Testing of Materials.
12. ASTM Test Method C1274-00, "Standard Test Method for Advanced Ceramic Specific Surface Area by Physical Adsorption," 2003, Annual Book of ASTM Standards, vol. 15.01, West Conshohocken, PA: American Society for the Testing of Materials.
13. ASTM Test Method E384-99e1, "Standard Test Method for Microindentation Hardness of Materials," 2004, Annual Book of ASTM Standards, vol. 03.01, West Conshohocken, PA: American Society for the Testing of Materials.
14. W.D. Kingery, "Role of Surface Energies and Wetting in Metal-Ceramic Sealing," *Ceramic Bulletin*, 1956, vol. 35, no. 3, pp. 108-12.
15. W.D. Kingery, H.K. Bowen, and D.R. Uhlmann, *Introduction to Ceramics*, 2d ed., 1976, New York, Wiley.
16. M.K. Stanford, A.M. Yanke, and C. DellaCorte, "Thermal Effects on a Low Cr Modification of PS304 Solid Lubricant Coating," 2004, NASA Technical Memorandum 213111, available at <http://gltrs.grc.nasa.gov/reports/2004/TM-2004-213111.pdf> (accessed October 25, 2004).
17. C. DellaCorte, "The Effects of Substrate Material and Thermal Processing Atmosphere on the Strength of PS304: A High Temperature Solid Lubricant Coating," 2003, *Tribology Transactions*, vol. 46, no. 3, pp. 361-68.

18. C. DellaCorte, B.J. Edmonds, and P.A. Benoy, "Thermal Processing Effects on the Adhesive Strength of PS304 High Temperature Solid Lubricant Coatings," 2001, NASA Technical Memorandum 210944, available at <http://gltrs.grc.nasa.gov/reports/2001/TM—2001-210944.pdf> (accessed October 25, 2004).
19. M.K. Stanford and C. DellaCorte, "Friction and Wear Characteristics of a Modified Composite Solid Lubricant Plasma Spray Coating," in *Surface Engineering: Proceedings of the 3rd International Surface Engineering Congress*, Narendra B. Dahotre and Oludele O. Popoola eds., ASM International, 2005, pp. 219–23.
20. P. Shewmon, *Diffusion in Solids*, 2d. ed., 1989, The Minerals, Metals & Materials Society, Warrendal, PA.
21. W.A. Johnson and R.F. Mehl, Reaction Kinetics in Processes of Nucleation and Growth, *Transactions of the Metallurgical Society of AIME*, 1939, vol. 135, pp. 416–43.
22. M. Avrami, Kinetics and Phase Change. I: General Theory, *Journal of Chemical Physics*, 1939, vol. 7, pp. 1103–12.
23. A.N. Kolmogorov, K statisticheskoi teorii kristallizatsii metallov (About statistical theory applied to metals crystallization), *Izvestiya Akademii Nauk SSSR: Seriya Matematicheskaya*, 1937, vol. 1, No. 3, pp. 355–59.
24. J.M. West, *Basic Corrosion and Oxidation*, Ellis Horwood Limited, Chichester, England, 1980.
25. M.G. Fontana, *Corrosion Engineering*, McGraw-Hill, Inc., 1986.
26. J.L. Smialek and G.H. Meier, "High Temperature Oxidation," *Superalloys II*, Chester T. Sims, Norman S. Stoloff, and W.C. Hagel eds., John Wiley & Sons, New York, 1987, pp. 293–326.

TABLE 1.—PM304 PRECOMPACTION POWDER
FEEDSTOCK CHARACTERISTICS

Composition	60 w/o Ni-20Cr 20 w/o Cr ₂ O ₃ 10 w/o Ag 10 w/o BaF ₂ -32CaF ₂
Size designation	–140 + 450 mesh (30 to 106 μm)
Apparent density	3.06±0.13 g/cm ³
Tap density	4.46±0.04 g/cm ³
Angle of repose	70.6°

TABLE 2.—MELTING TEMPERATURES AND PURITY
LEVELS OF THE CONSTITUENT MATERIALS

Constituent	Melt Point (°C)	Purity
Ni-20 w/o Cr	1400	98.17%
Cr ₂ O ₃	2330 (sublimes)	99.18%
Ag	960	> 99%
BaF ₂ -32 w/o CaF ₂	1050	> 99%



Figure 1.—Typical PM300 bushings used in this investigation.

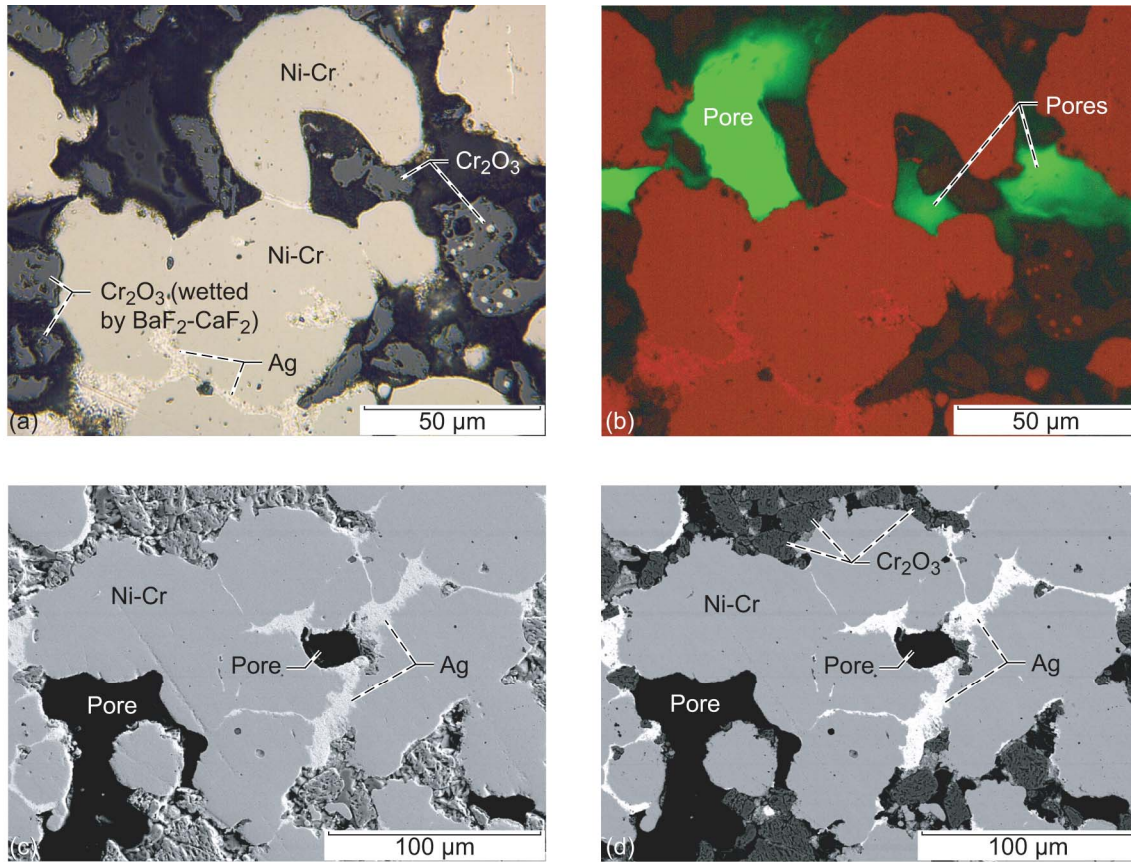


Figure 2.—PM300 self-lubricating composite shown with (a) brightfield and (b) polarized optical photomicrographs from the same area on the specimen as well as (c) secondary and (d) backscattered electron images from another area on the same specimen with 25 kV accelerating voltage (500× original magnification). Note results of liquid phase sintering where Ag wets Ni-Cr. Likewise, $\text{BaF}_2\text{-CaF}_2$ surrounds faceted Cr_2O_3 particles.

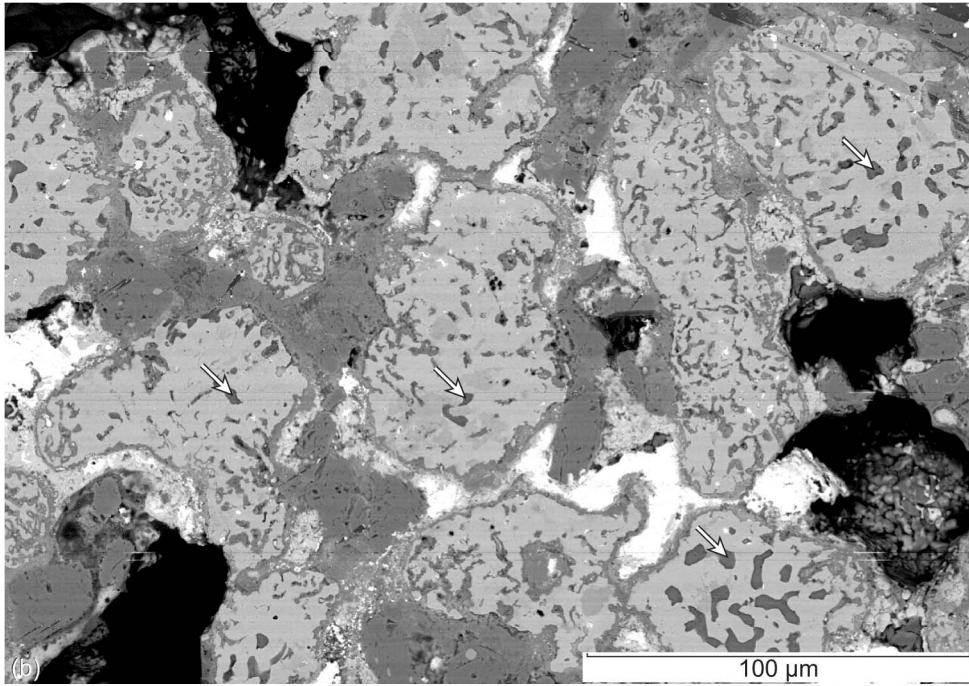
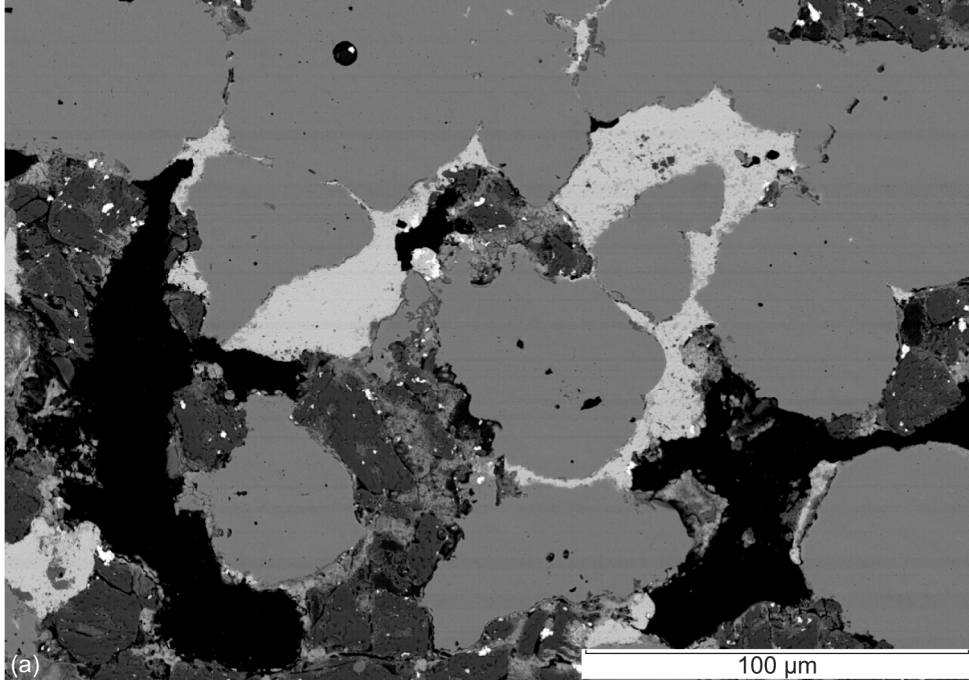


Figure 3.—Backscattered SEM photomicrographs (25 kV accelerating voltage) of PM300 after exposure to (a) 500 and (b) 650 °C in air for 100 h (500× original magnification). Precipitates are clearly visible in the specimen exposed to 650 °C (some indicated with arrows).

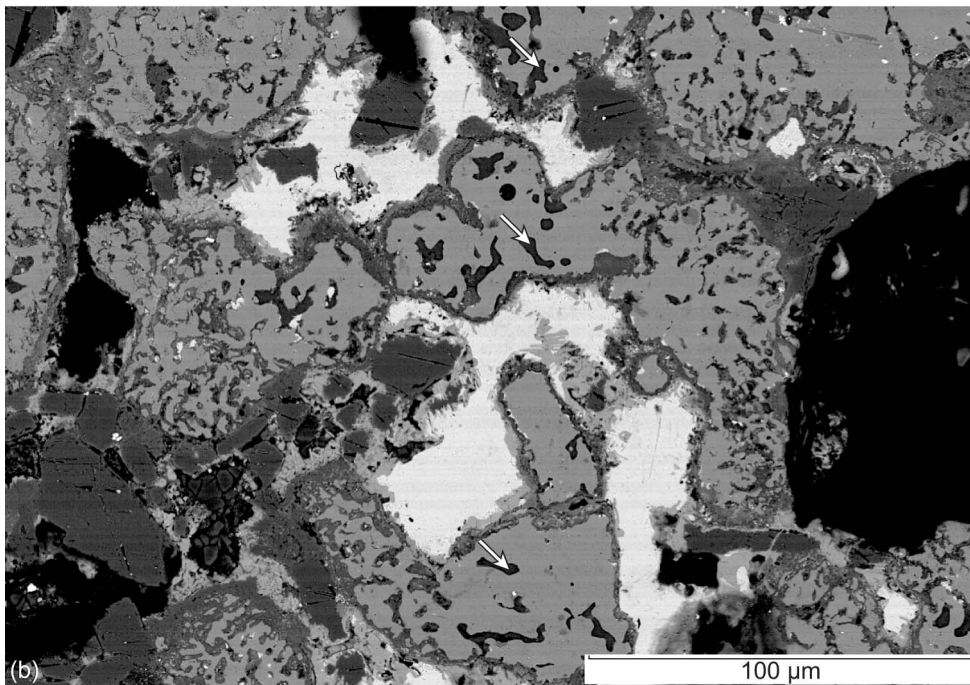
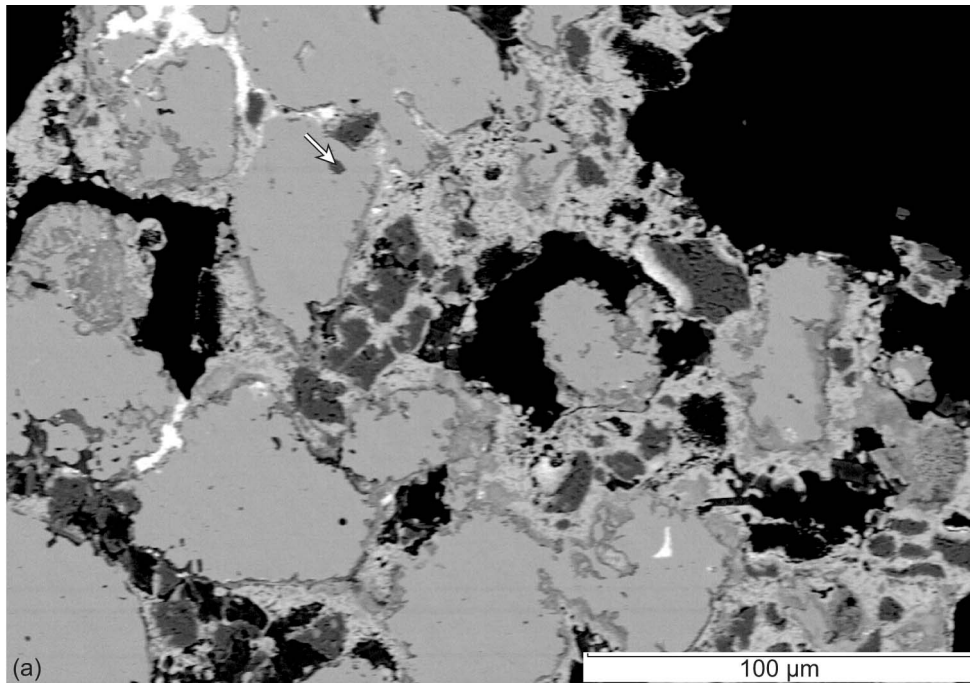


Figure 4.—Backscattered SEM photomicrographs (25 kV accelerating voltage) of PM300 after exposure to (a) 500 and (b) 650 °C in air for 500 h (500× original magnification). Few precipitates are visible in the specimen exposed to 500 °C while there are many precipitates in the 650 °C specimen (several precipitates indicated with arrows).

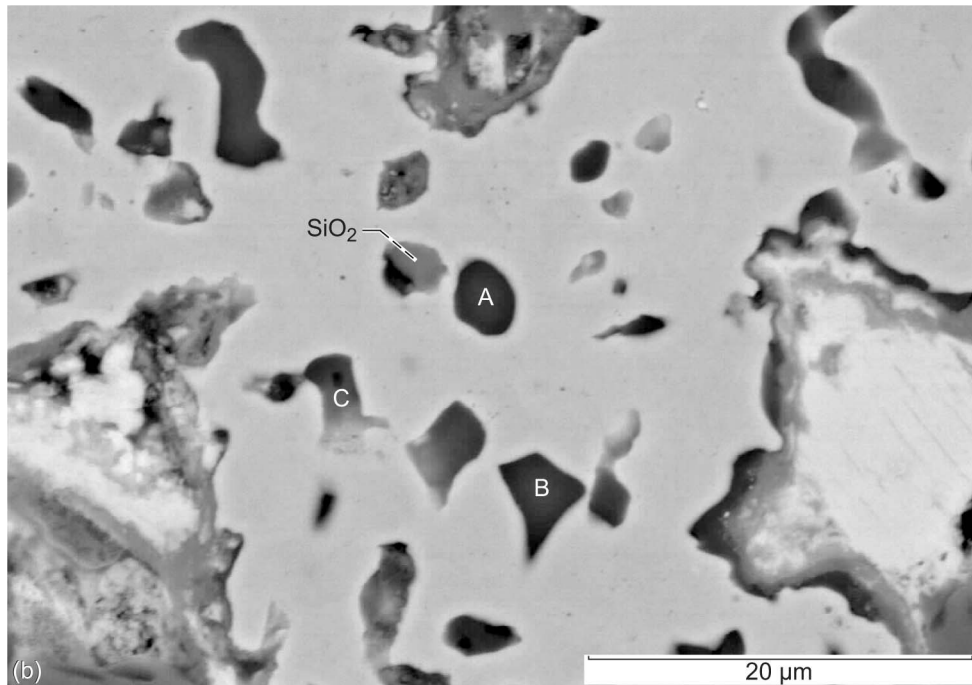
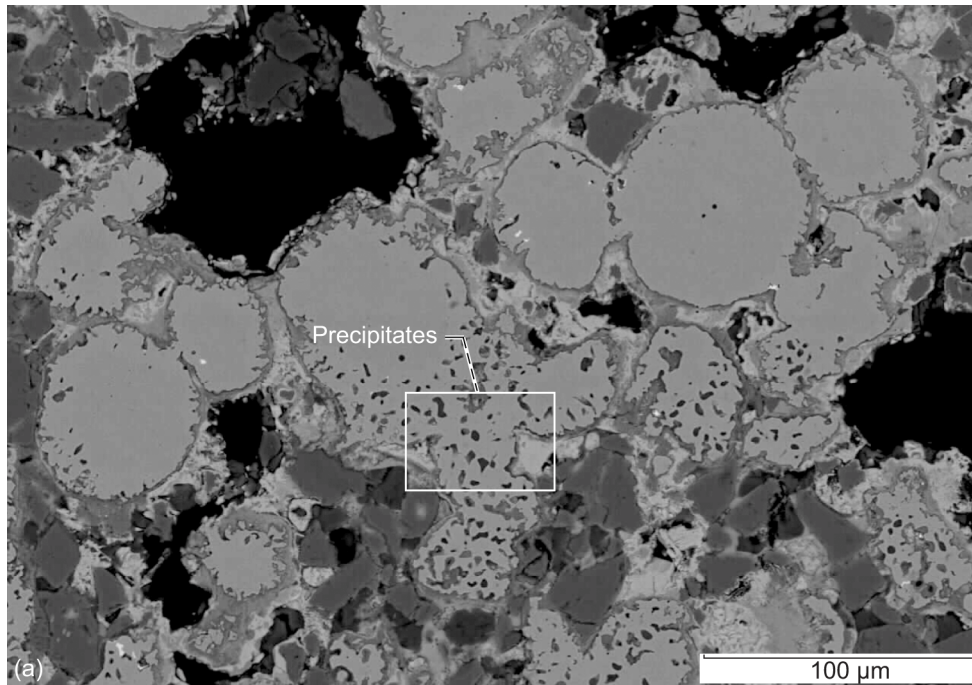


Figure 5.—Backscattered SEM images of precipitates in PM300 specimen exposed to 500 °C for 5,000 h at (a) 350× and (b) 2,500× original magnification (25 kV accelerating voltage). The SiO₂ particle is contamination, possibly from the metallographic procedure.

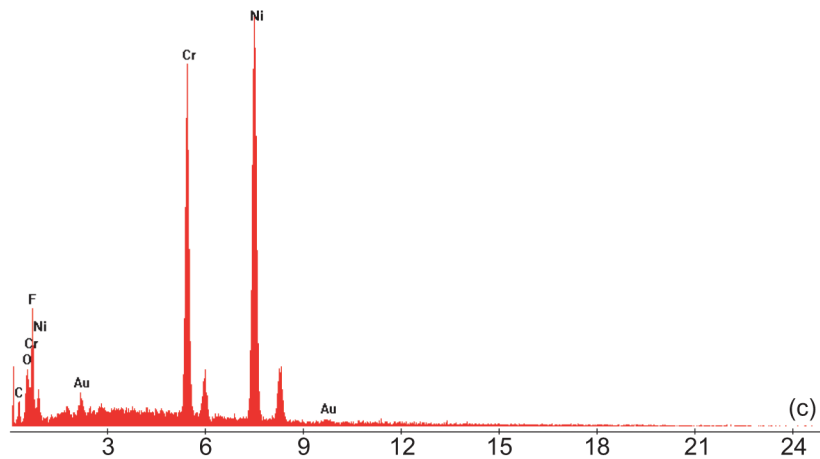
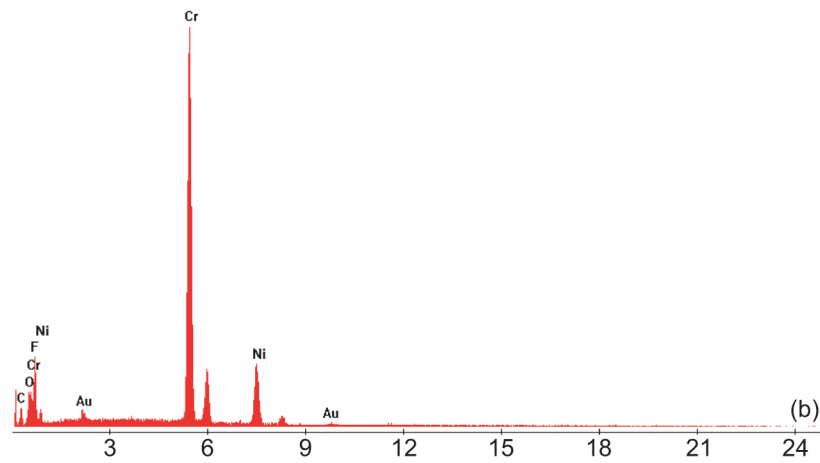
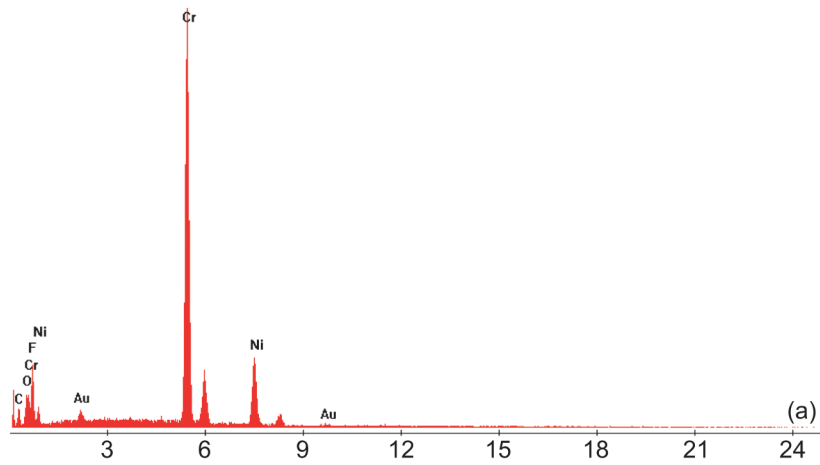


Figure 6.—EDS spectra with 25 kV accelerating voltage of precipitates in PM300 specimen exposed to 500 °C for 5,000 h at (a) point A, (b) point B and (c) point C (as specified in figure 5b). The weak Au peaks in these spectra are due to the thin conductive film.

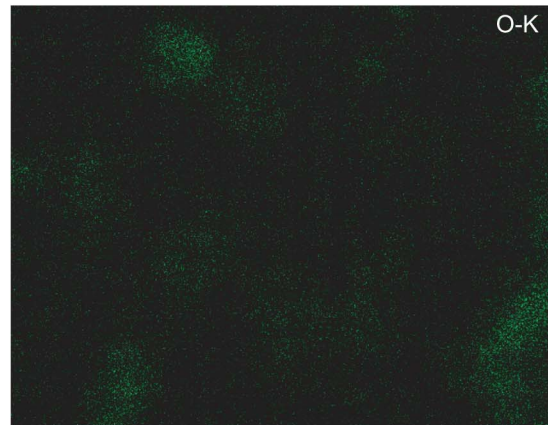
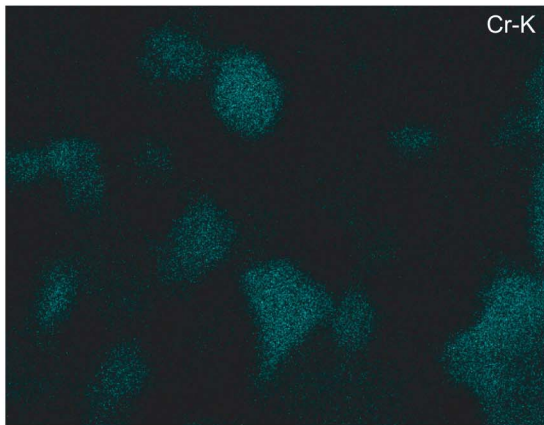
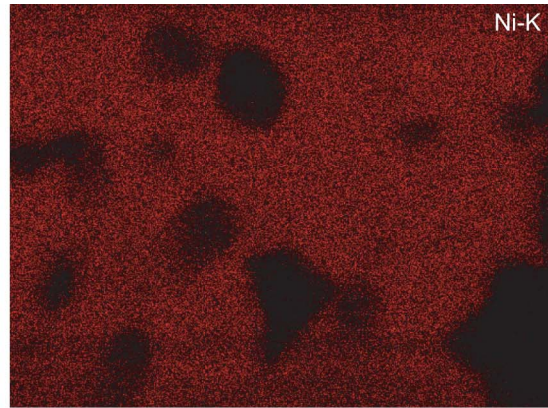
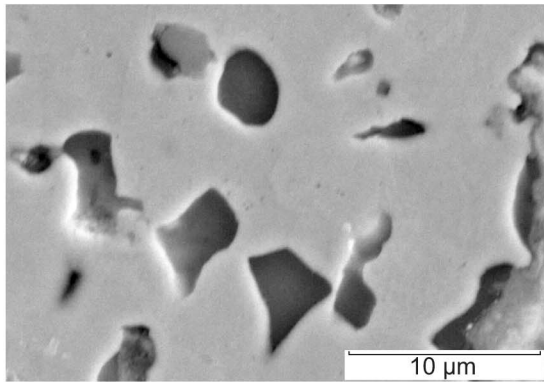


Figure 7.—Elemental dot maps from PM300 specimen (as shown in figure 5) exposed to 500 °C for 5,000 h (4,500× original magnification). Analysis performed at 25 kV.

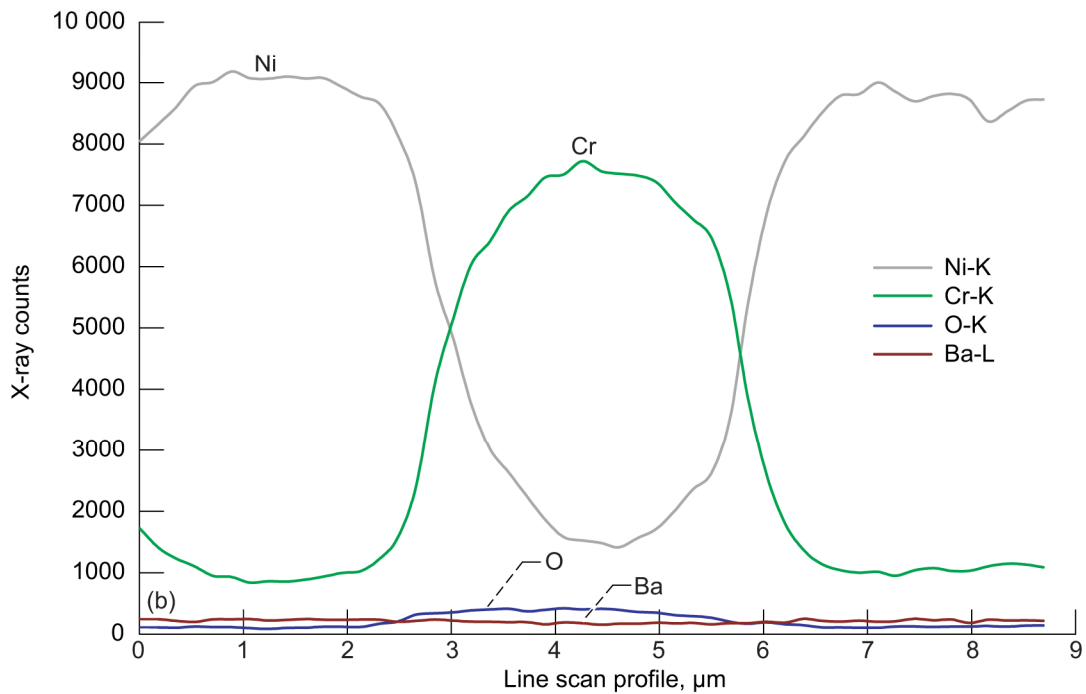
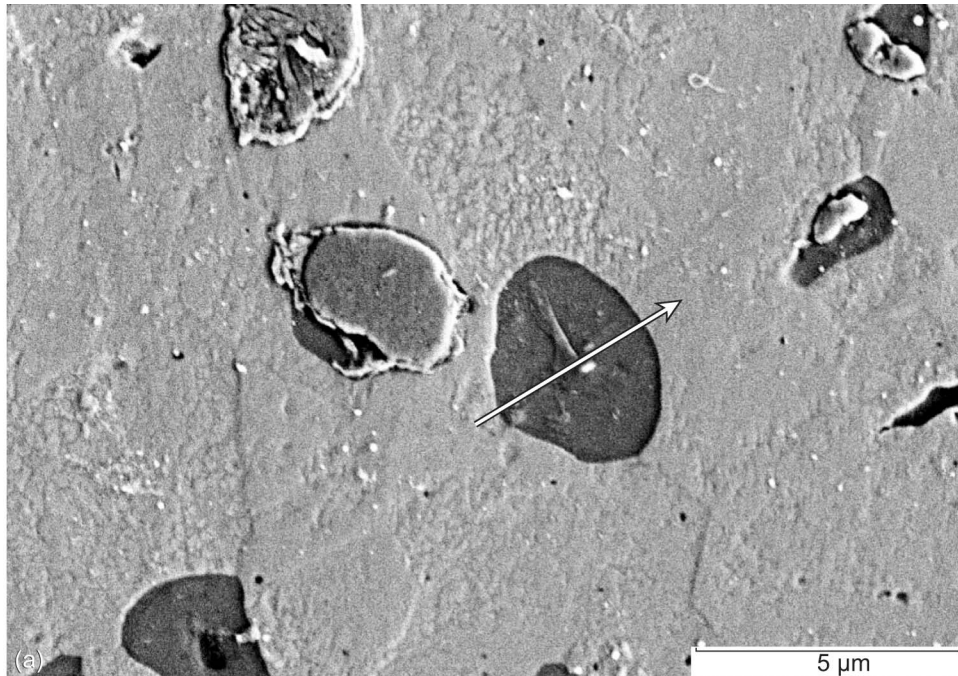


Figure 8.—Secondary electron SEM photomicrograph (7,000× original magnification) and elemental line scan of cross-section shown in figure 5 (precipitate in PM300 specimen exposed to 500 °C for 5,000 h). The arrow in the photomicrograph indicates direction of line scan. Analysis performed at 6 kV.

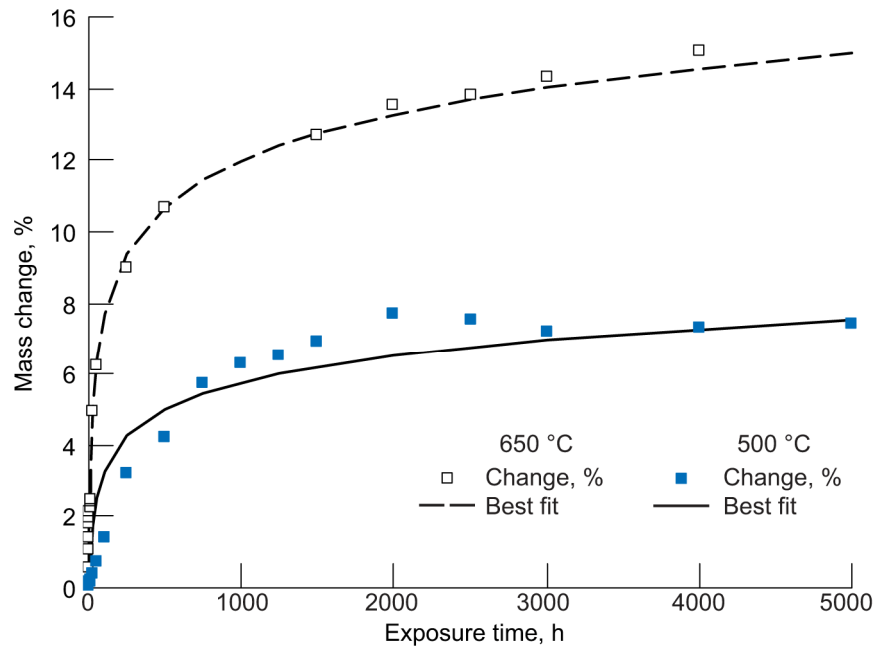


Figure 9.—Plot of PM300 percent mass change versus time at 500 and 650 °C.

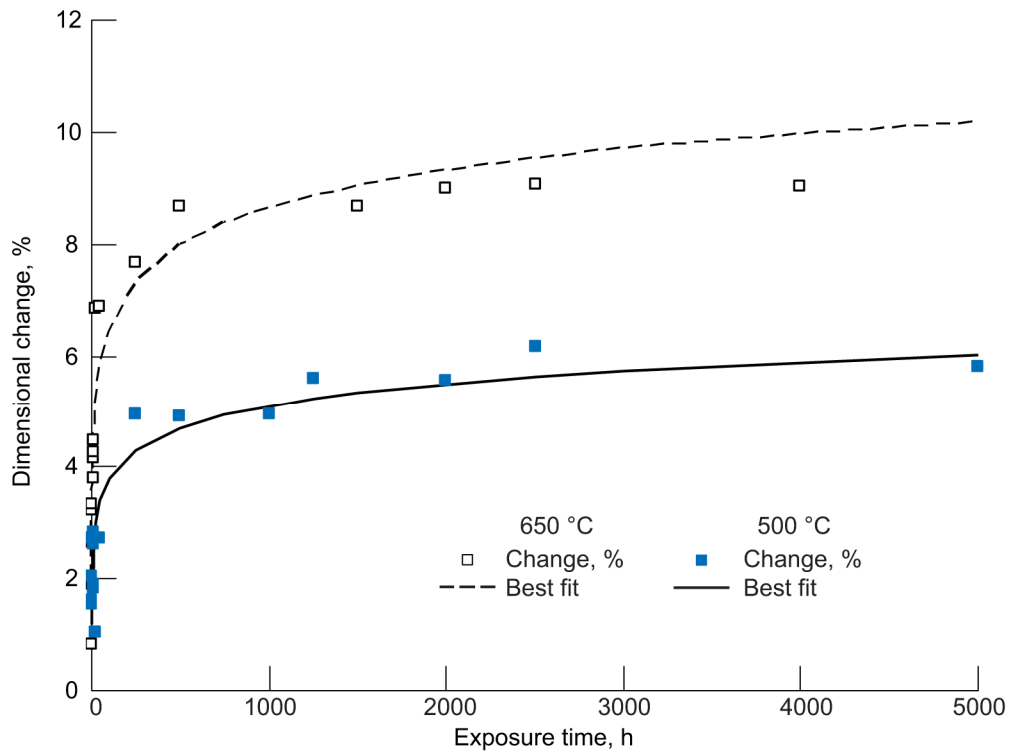


Figure 10.—Plot of PM300 dimensional change versus time at 500 and 650 °C.

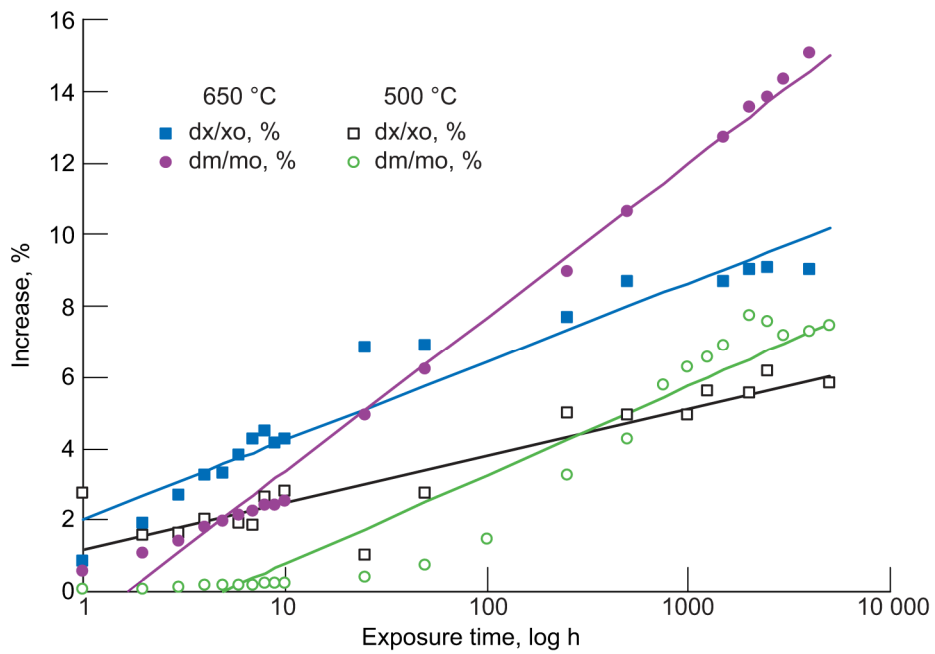


Figure 11.—Plot combining mass and dimension increase data from figures 9 and 10.

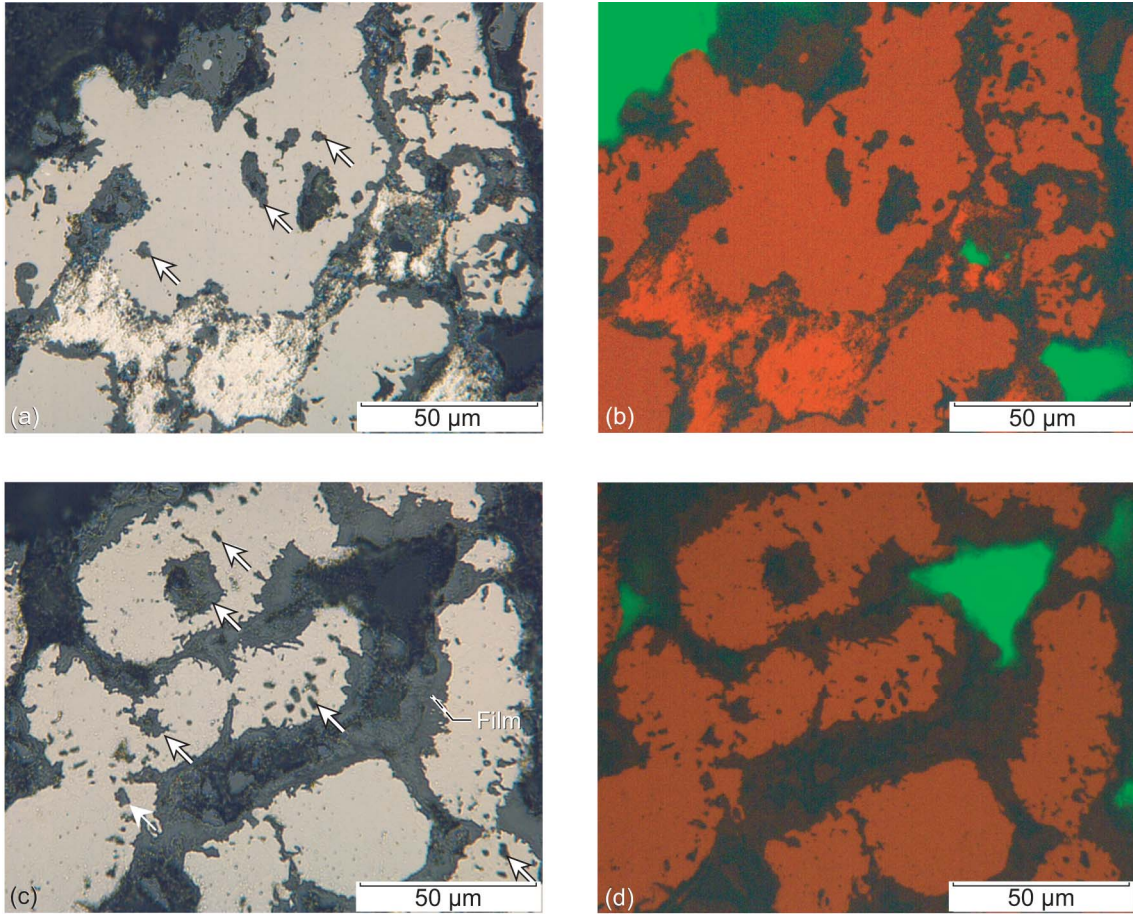


Figure 12.—Optical photomicrographs (500× original magnification) of PM300 showing increase of precipitates (highlighted with arrows) after 500 h at 500 °C. Images on left (a and c) are brightfield photomicrographs, while images on right (b and d) were captured through a fluorescent filter. Note the film that is forming on edges of Ni-Cr constituent.

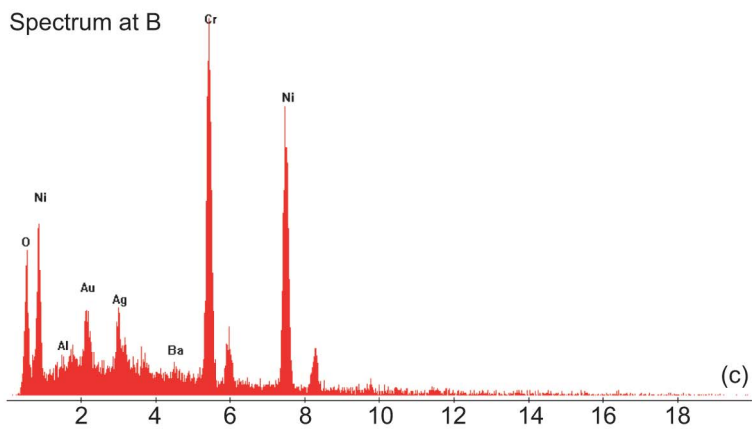
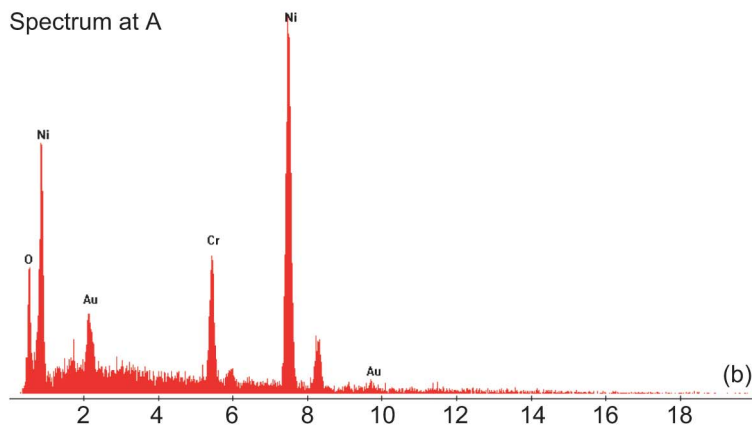
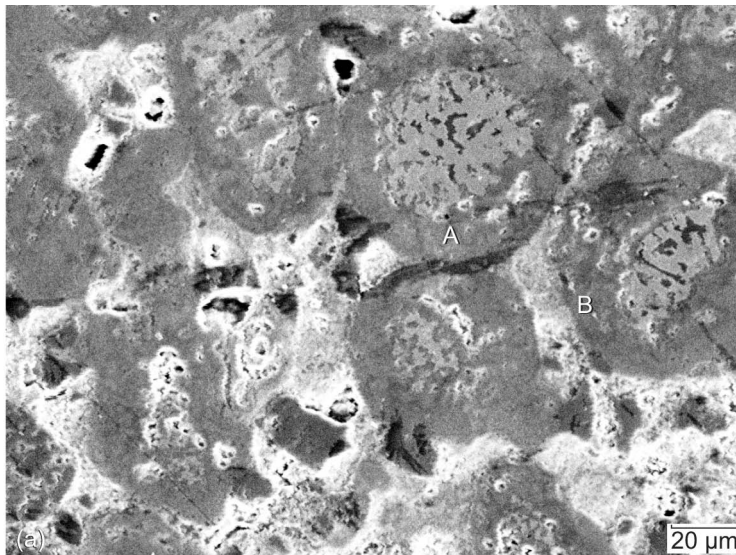


Figure 13.—Backscattered SEM image with analysis of oxide film developing on Ni-Cr particle after exposure to 650 °C for 3,000 h (20 kV accelerating voltage); the composition at points A and B are shown in the corresponding spectra.

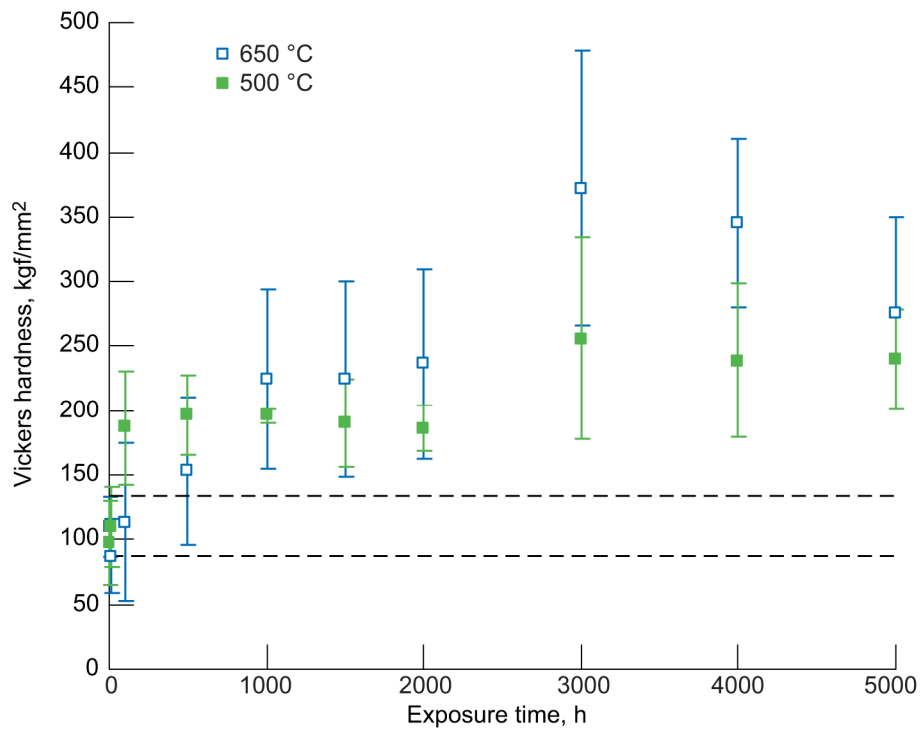


Figure 14.—Plot of microindentation hardness versus time of exposure to 500 and 650 °C.

REPORT DOCUMENTATION PAGEForm Approved
OMB No. 0704-0188

Public reporting burden for this collection of information is estimated to average 1 hour per response, including the time for reviewing instructions, searching existing data sources, gathering and maintaining the data needed, and completing and reviewing the collection of information. Send comments regarding this burden estimate or any other aspect of this collection of information, including suggestions for reducing this burden, to Washington Headquarters Services, Directorate for Information Operations and Reports, 1215 Jefferson Davis Highway, Suite 1204, Arlington, VA 22202-4302, and to the Office of Management and Budget, Paperwork Reduction Project (0704-0188), Washington, DC 20503.

1. AGENCY USE ONLY (Leave blank)		2. REPORT DATE February 2006	3. REPORT TYPE AND DATES COVERED Technical Memorandum	
4. TITLE AND SUBTITLE Effect of Prolonged Exposure to High Temperature Air on Physical Characteristics of a Powder Metallurgy Composite Solid Lubricant			5. FUNDING NUMBERS WBS-22-714-09-15	
6. AUTHOR(S) Malcolm K. Stanford, La'Nita D. Ward, and Christopher Dellacorte				
7. PERFORMING ORGANIZATION NAME(S) AND ADDRESS(ES) National Aeronautics and Space Administration John H. Glenn Research Center at Lewis Field Cleveland, Ohio 44135-3191			8. PERFORMING ORGANIZATION REPORT NUMBER E-15070	
9. SPONSORING/MONITORING AGENCY NAME(S) AND ADDRESS(ES) National Aeronautics and Space Administration Washington, DC 20546-0001			10. SPONSORING/MONITORING AGENCY REPORT NUMBER NASA TM-2006-213603	
11. SUPPLEMENTARY NOTES Malcolm K. Stanford and Christopher DellaCorte, Glenn Research Center; La'Nita D. Ward, Spelman College, 350 Spelman Lane, Atlanta, Georgia 30314. Responsible person Malcolm K. Stanford, organization code RST, 216-433-3387.				
12a. DISTRIBUTION/AVAILABILITY STATEMENT Unclassified - Unlimited Subject Category: 26 Available electronically at http://gltrs.grc.nasa.gov This publication is available from the NASA Center for AeroSpace Information, 301-621-0390.			12b. DISTRIBUTION CODE	
13. ABSTRACT (Maximum 200 words) The effects of exposure to high temperatures has been investigated for PM300, a powder metallurgy composite solid lubricant composed of nickel-chromium, chromia, silver, and an alkaline earth fluoride. Specimens were exposed to 500 and 650 °C in air for time intervals up to 5,000 hr and then examined for changes in their microstructure, mass, size, and hardness. After heat exposure, the microstructure showed formation of precipitates within the nickel-chromium constituent, with a corresponding increase in mass, size, and hardness. The percent increase in mass and size followed a logarithmic curve, which provides guidance for heat treatment parameters.				
14. SUBJECT TERMS Powder metallurgy; Composite materials; Solid lubricants; Oxidation; Microstructure; Thickness; Vickers hardness			15. NUMBER OF PAGES 26	
			16. PRICE CODE	
17. SECURITY CLASSIFICATION OF REPORT Unclassified	18. SECURITY CLASSIFICATION OF THIS PAGE Unclassified	19. SECURITY CLASSIFICATION OF ABSTRACT Unclassified	20. LIMITATION OF ABSTRACT	

